

<https://doi.org/10.1038/s42003-025-08167-9>

TRPV2 mediates stress resilience in mouse cardiomyocytes

Check for updates

Yubing Dong^{1,2}, Guohao Wang¹, Yoshihiro Ujihara³, Yan Zhu Chen^{1,2}, Masashi Yoshida⁴, Kazufumi Nakamura^{5,6}, Kimiaki Katanosaka⁷, Keiji Naruse¹ & Yuki Katanosaka^{1,2}

The heart dynamically compensates for haemodynamic stress, but how this resilience forms during cardiac growth is not clear. Using a temporally inducible, cardiac-specific knockout in mice we show that the Transient receptor potential vanilloid family 2 (TRPV2) channel is crucial for the maturation of cardiomyocyte stress resilience. TRPV2 defects in growing hearts lead to small morphology, abnormal intercalated discs, weak contractility, and low expression of serum response factor and Insulin-like growth factor-1 (IGF-1) signalling. Individual cardiomyocytes of TRPV2-deficient hearts show reduced contractility with abnormal Ca^{2+} handling. In cultured neonatal cardiomyocytes, mechanical Ca^{2+} response, excitation–contraction coupling, sarcoplasmic reticulum Ca^{2+} content, actin formation, nuclear localisation of Myocyte enhancer factor 2c, and IGF-1 expression require TRPV2. TRPV2-deficient hearts show a defective response to dobutamine stress and no compensatory hypertrophic response to phenylephrine administration, but no stress response to pressure overload. These data suggest TRPV2 mediates the maturation of cardiomyocyte stress resilience, and will advance therapeutic interventions and drug discovery for heart disease.

Maturation is the last phase of cardiac development and prepares the heart for strong, efficient pumping throughout life¹. Cardiomyocyte maturation ensures cardiac integrity and increases the pumping function of the heart. The processes underlying cardiac maturation, including cellular and organ growth and electrophysiological, metabolic, and contractile maturation, are complex, and it remains unclear how these processes are integrated and interact to produce mature myocardium^{1,2}. Mature hearts are known to induce an adult-like phenotype in immature cardiomyocytes that are transplanted *in vivo*, but the mechanism for this also remains unclear³. Elucidation of the cardiomyocyte maturation process is, therefore, an important issue for regenerative medicine and studies of remodelling in the context of heart failure pathology.

The heart changes its shape and function in response to haemodynamic load, but it is not clear how this resilience is formed during the cardiomyocyte maturation process⁴. Cyclic mechanical stress during systole and passive stretch during diastole trigger changes in gene expression and remodelling of myocyte morphology and structure to generate a mature appearance¹, but the mechanism of mechanotransduction in cardiomyocytes has not been elucidated, so it is not clear how mechanical stress triggers

cardiomyocyte remodelling. Piezo1 is a mechanosensitive channel that is expressed in the sarcolemma of cardiomyocytes; however, mice with cardiac-specific Piezo1 knockout showed normal heart structure and function in adulthood, suggesting that Piezo1 is not involved in embryonic development or postnatal growth of the heart^{5–9}. In another group of experiments, tamoxifen-inducible, cardiomyocyte-specific Piezo1 knockout did not affect cardiac structure and function under physiological conditions in adult mice, indicating that the role of Piezo1 in cardiomyocyte maintenance is also minimal¹⁰.

The mechanoreception that enables cardiomyocytes to respond to tension, flow, or changes in cell volume might be provided by members of the transient receptor potential (TRP) family of cation channels¹¹, which play a key role in pressure overload-induced pathological heart remodelling¹². TRPC3 or TRPC6 deficiency was reported to suppress pressure overload-induced cardiac fibrosis, but not myocyte hypertrophic responses, in mice^{13,14}, and TRPV4 was reported to be involved in pressure overload-induced hypertrophy and fibrosis¹⁵. The systemic-knockout mice used in those experiments showed no abnormalities in cardiac function or morphology under physiological conditions, so the contributions of

¹Department of Cardiovascular Physiology, Graduate School of Medicine, Dentistry and Pharmaceutical Sciences, Okayama University, Okayama, Japan.

²Department of Pharmacy, College of Pharmacy, Kinjo Gakuin University, Nagoya, Aichi, Japan. ³Department of Electrical and Mechanical Engineering, Graduate School of Engineering, Nagoya Institute of Technology, Nagoya, Aichi, Japan. ⁴Department of Chronic Kidney Disease and Cardiovascular Disease, Okayama University Faculty of Medicine, Dentistry and Pharmaceutical Sciences, Okayama, Japan. ⁵Department of Cardiovascular Medicine, Okayama University Faculty of Medicine, Dentistry and Pharmaceutical Sciences, Okayama, Japan. ⁶Center for Advanced Heart Failure, Okayama University Hospital, Okayama, Japan.

⁷Department of Biomedical Sciences, College of Life and Health Sciences, Chubu University, Kasugai, Aichi, Japan. e-mail: katanosaka@kinjo-u.ac.jp

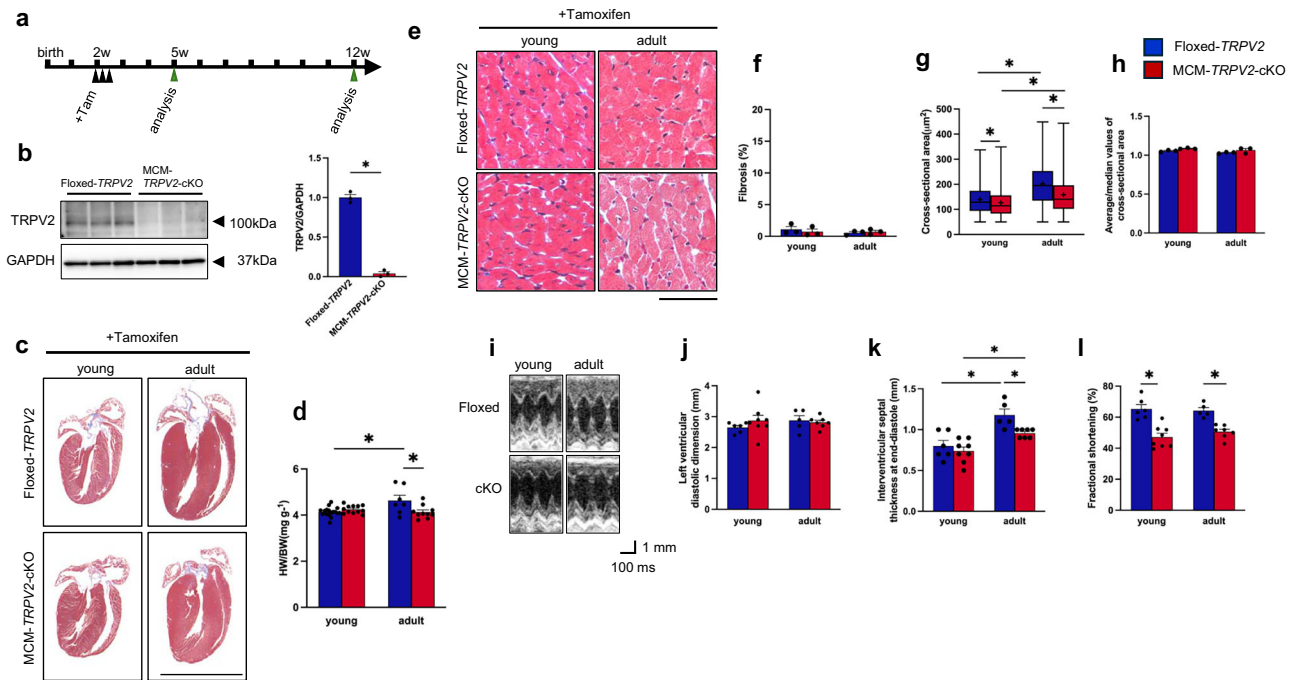


Fig. 1 | Cardiac changes after removal of TRPV2 from a young age. **a** Schedule of tamoxifen administration. **b** Expression of TRPV2 protein in tamoxifen-treated heart at 5 weeks ($N = 3$). **c** Cardiac morphology (scale bar, 5 mm). **d** Changes in heart-to-body weight (HW/BW) ratio ($N = 7-17$ mice per group). **e** Masson's trichrome staining of the left ventricle. Scale bar, 50 μm . **f** Fibrosis percentage. **g, h** Changes in cross-sectional area of cardiomyocytes ($n = 723-995$ cells from 3

mice per group). **i** Representative tracing of two-dimensional transthoracic M-mode echocardiography. **j-l** Echocardiographic assessment of left ventricular end dimension at systole, interventricular septal thickness at end-diastole, and fractional shortening ($N = 5-8$ mice per group). Data are shown as mean \pm standard error of the mean (SEM). * $P < 0.05$ between indicated groups based on Tukey-Kramer test.

TRPC3, TRPC6, and TRPV4 channels to cardiomyocyte maturation are probably low.

Previously, we reported that recombinant TRP vanilloid family type 2 (TRPV2) channels can be activated by hypotonicity- or stretch-induced mechanical stimulation in ectopic expression systems¹⁶⁻¹⁸. Furthermore, we showed that cardiac-specific elimination of TRPV2 led to severe cardiac dysfunction, with disorganisation of intercalated discs that support mechanical and electrical coupling between neighbouring myocytes, as well as downregulation of Insulin-like growth factor 1 receptor (IGF1R)/Phosphatidylinositol-3 kinase (PI3K)/Akt signalling, which is crucial for myocyte maturation¹⁸. In another group of experiments, mice with systemic TRPV2 knockout showed reduced cardiac function under physiological conditions¹⁹. These findings suggest that TRPV2 regulates signalling pathways involved in cardiomyocyte maturation and plays an important role in increasing heart contractility during growth.

In the present study, we used mice with temporally controlled, cardiac-specific conditional TRPV2 knockout to evaluate the role of TRPV2 in postnatal heart growth and cardiomyocyte maturation. When cardiac-specific TRPV2 knockout was applied in juvenile mice and the mice were subsequently grown to adulthood, their hearts displayed small morphology, weak contractility, and low expression of Sarcoendoplasmic reticulum Ca^{2+} -ATPase (SERCA2a) and molecules related to Serum response factor (SRF)/Insulin-like growth factor 1 (IGF-1) signalling. Furthermore, these TRPV2-deficient hearts showed altered localisation of Ca^{2+} regulatory proteins and reduced contractility of isolated cardiomyocytes. Although IGF-1 expression is TRPV2 dependent, administration of IGF-1 alone did not induce hypertrophic correction, suggesting that the TRPV2 signal is important for cardiomyocyte maturation and physiological hypertrophy. Dobutamine stress test and chronic phenylephrine (PE) administration in TRPV2-deficient hearts indicated that TRPV2 is crucial for maturation of stress-responsive capacity during cardiac growth. In addition, TRPV2-deficient hearts showed no structural or functional changes in response to pressure overload, suggesting that TRPV2 is a key member of the mechanosensitive

system of cardiomyocytes. These results suggest that TRPV2 is crucial for the maturation of cardiomyocyte stress resilience, and this signal is reflected in mechanical feedback in the beating heart.

Results

Cardiac-specific elimination of TRPV2 in young mice resulted in changes in heart morphology and function in adulthood

To examine the role of TRPV2 in cardiac growth and maturation, we injected tamoxifen into the abdominal cavity of 2-week-old $\text{TRPV2}^{\text{flo}/\text{lox}}$; $\text{MerCreMer}^{-/-}$ (Floxed-TRPV2) mice and $\text{TRPV2}^{\text{flo}/\text{lox}}$; $\text{MerCreMer}^{+/-}$ (MCM-TRPV2-cKO) mice for 3 consecutive days (Fig. 1a). The successful recombination of the TRPV2 gene after tamoxifen administration was confirmed by PCR (Supplementary Fig. 1). TRPV2 expression in the hearts of 5-week-old MCM-TRPV2-cKO mice treated with tamoxifen was reduced by approximately 95% compared with that in the hearts of Floxed-TRPV2 mice under the same conditions (Fig. 1b). After TRPV2 was conditionally knocked out at 2 weeks of age, the resulting morphological and functional changes in the heart were analysed at 5 and 12 weeks of age (Fig. 1a). The survival rate of tamoxifen-treated MCM-TRPV2-cKO mice was over 90%, comparable to that of MCM-TRPV2-cKO mice without tamoxifen or Floxed-TRPV2 mice with or without tamoxifen (Floxed-TRPV2 with vehicle, 93.02% $N = 129$; Floxed-TRPV2 with tamoxifen, 91.60%, $N = 131$; TRPV2-cKO with vehicle, 92.36%; $N = 131$; TRPV2-cKO with tamoxifen, 92.68%, $N = 123$). In this study, we defined 5-week-old mice as young and 12-week-old mice as adults. In young mice, there was no difference in cardiac morphology or heart-weight-to-body-weight ratio between Floxed-TRPV2 mice and MCM-TRPV2-cKO mice (Fig. 1c, d). By contrast, the hearts of adult MCM-TRPV2-cKO mice were similar to those of young mice and were clearly smaller than those of adult Floxed-TRPV2 mice, which had grown larger than their young counterparts (Fig. 1c, d). There was no fibrosis evident in the hearts of Floxed-TRPV2 mice or MCM-TRPV2-cKO mice (Fig. 1e, f). An analysis of the cross-sectional area of isolated cardiomyocytes showed that cardiomyocytes of adult MCM-TRPV2-cKO mice

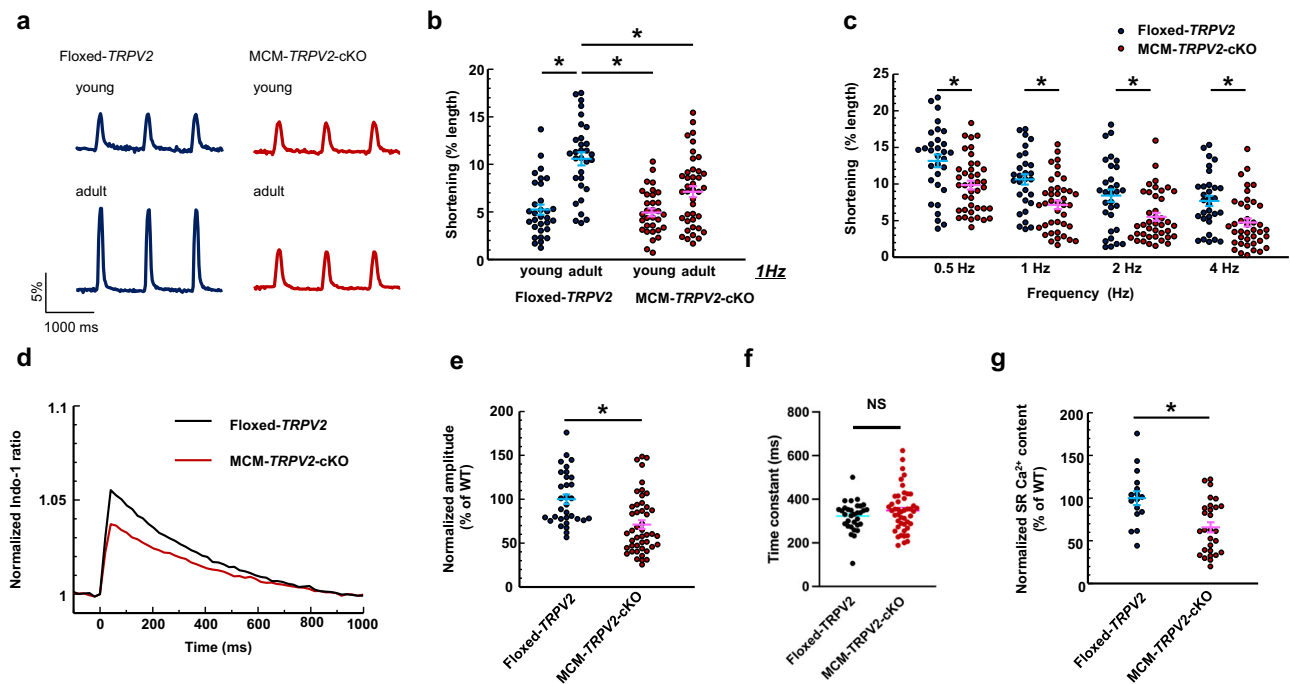


Fig. 2 | Changes in contractility and Ca^{2+} handling of MCM-TRPV2-cKO cardiomyocytes. **a** Representative tracing of myocyte shortening. **b** Change in contractility at 1 Hz in young and adult myocytes ($n = 31$ –40 cells from three hearts per group). * $P < 0.05$ between indicated groups based on Tukey–Kramer test. **c** Frequency-dependent shortening of cardiomyocytes ($n = 31$ –40 cells from three hearts per group). * $P < 0.05$ vs. tamoxifen-treated floxed cells at the same frequency

based on Student's t -test. **d** Representative trace of Indo-1 fluorescence in single cardiomyocytes stimulated at 1 Hz. **e** Peak amplitude of Ca^{2+} transients ($n = 32$ –46 cells from three hearts per group). **f** Decay time constant (obtained by fitting the decline phase). **g** Estimation of sarcoplasmic reticulum Ca^{2+} content ($n = 16$ –28 cells from three hearts per group). * $P < 0.05$ vs. tamoxifen-treated floxed cells based on Student's t -test. Data are shown as mean \pm standard error of the mean (SEM).

were larger than those of young MCM-TRPV2-cKO mice but clearly smaller than those of adult Floxed-TRPV2 mice (Fig. 1g, h), suggesting that elimination of TRPV2 attenuated cardiomyocyte growth. Echocardiographic analysis revealed no abnormalities in left ventricular end-diastolic diameter, but lower contractility in MCM-TRPV2-cKO hearts than in Floxed-TRPV2 hearts, regardless of age (Fig. 1i–l). These results suggest that TRPV2 is crucial for structural and functional growth of the heart.

Individual MCM-TRPV2-cKO cardiomyocytes displayed reduced contractility and impaired Ca^{2+} handling

To determine whether the reduced cardiac function in MCM-TRPV2-cKO mice was due to impaired function of individual cardiomyocytes, we examined the contractility and Ca^{2+} handling with excitation–contraction (E–C) coupling of isolated cardiomyocytes. There was no difference in cardiomyocyte contractility between young MCM-TRPV2-cKO mice and young Floxed-TRPV2 mice; however, cardiomyocyte contractility was significantly higher in adult Floxed-TRPV2 mice than in adult MCM-TRPV2-cKO mice, which had almost the same cardiomyocyte contractility as young MCM-TRPV2-cKO mice (Fig. 2a, b). Furthermore, compared with cardiomyocytes from adult Floxed-TRPV2 mice, cardiomyocytes from adult MCM-TRPV2-cKO mice had a lower amplitude of electrical stimulation-dependent Ca^{2+} transients (Fig. 2c–f) and lower sarcoplasmic reticulum (SR) Ca^{2+} contents, as determined by caffeine-dependent Ca^{2+} release (Fig. 2g). These results suggest that the reduced cardiac function in adult MCM-TRPV2-cKO mice was due to impairment of individual cardiomyocytes.

Loss of TRPV2 altered the expression and localisation of Ca^{2+} regulators involved in E–C coupling

In cardiomyocytes, Ca^{2+} regulatory proteins display subcellular localisation and expression that are well suited to their cellular functions^{18,20,21}. Because systolic Ca^{2+} release occurs at the dyad, which consists of the T-tubule and

SR membranes, we analysed the localisation of Ca^{2+} transporters and junctophilin-2 (JP2), which helps to coordinate these structures. In adult Floxed-TRPV2 hearts, L-type Ca^{2+} channels (LTCC) and $\text{Na}^+/\text{Ca}^{2+}$ exchanger 1 (NCX1) were localised in T-tubules, and SERCA2a and JP2 were located on SR membranes, such that immunofluorescence signals appeared as well-ordered, ladder-like patterns (Fig. 3a, upper panels). However, in adult MCM-TRPV2-cKO hearts, the localisation of Ca^{2+} transporters and JP2 was disordered, with no clear ladder-like pattern (Fig. 3a, second-row panels from top). In young mice, the localisation of Ca^{2+} transporters and JP2 was not clear, but there was no difference between MCM-TRPV2-cKO hearts and Floxed-TRPV2 hearts (Fig. 3a, bottom two rows of panels). These results suggest that TRPV2 has an important role in the development of the dyad structure, and that the impaired contractility and Ca^{2+} handling in MCM-TRPV2-cKO cardiomyocytes might be due to abnormal dyad function caused by disrupted localisation of Ca^{2+} transporters involved in E–C coupling.

During postnatal cardiac growth, responsibility for the function of Ca^{2+} efflux from the intracellular space shifts from NCX1 to SERCA2a^{22,23}. Therefore, we analysed changes in the expression of Ca^{2+} transporters and JP2 that occurred during the postnatal growth of Floxed-TRPV2 and MCM-TRPV2-cKO hearts. There was no significant difference in the expression of LTCC, NCX1, or JP2 between Floxed-TRPV2 hearts and MCM-TRPV2-cKO hearts, regardless of age (Fig. 3b–e); however, SERCA2a expression was severely reduced in young MCM-TRPV2-cKO hearts, and this reduction was significantly reversed in adult MCM-TRPV2-cKO hearts (Fig. 3b, f). Notably, the myofibers of adult MCM-TRPV2-cKO hearts had markedly disorganised, thin, weak Z-bands (white arrowheads) and less mature sarcomere structures compared with the myofibers of adult Floxed-TRPV2 hearts (Fig. 3g). These results suggest that TRPV2 has a major impact on SERCA2a expression during cardiac growth and plays a crucial role in the development of contractile function by regulating SERCA2a expression and sarcomere integrity.

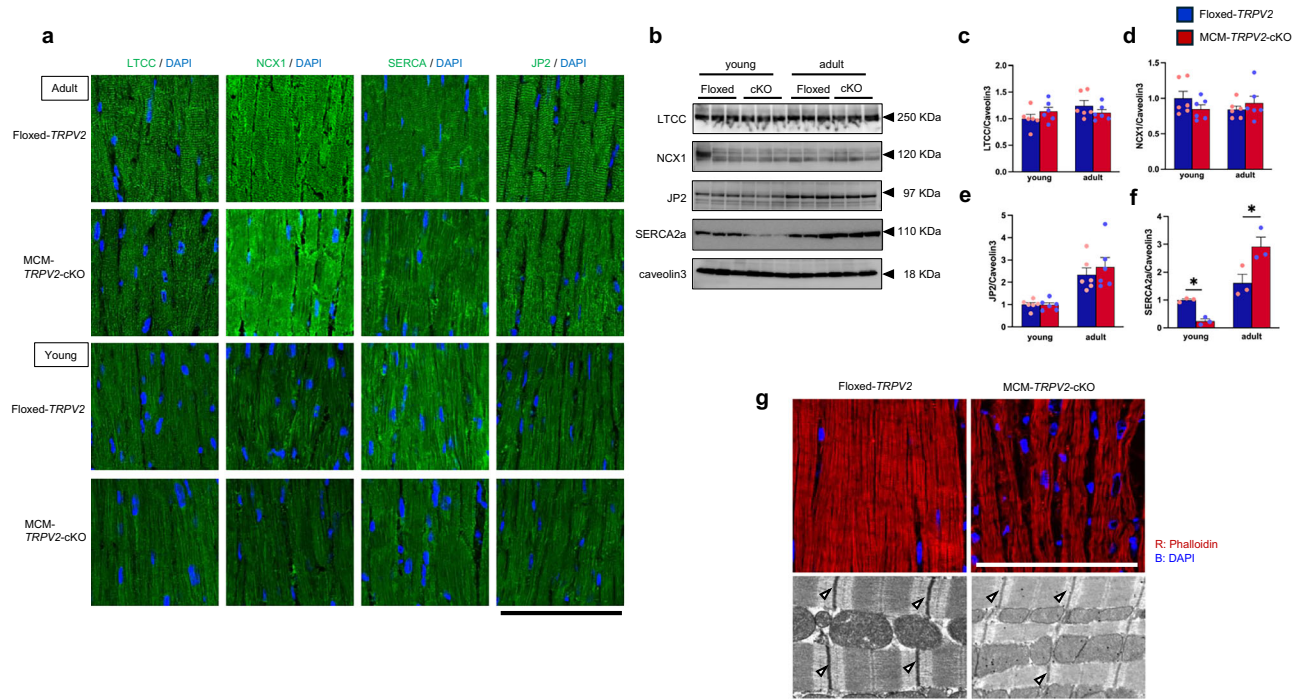


Fig. 3 | Expression of Ca^{2+} handling proteins in young and adult MCM-TRPV2-cKO hearts. **a** Change in localisation of LTCC, NCX1, SERCA, and JP2 in young and adult hearts. Double staining of the antibody of target protein (Green) and DAPI (blue). Scale bar, 100 μm . **b–f** Representative immunoblots (**c**) and expression level (**d–f**) of LTCC, NCX1, SERCA, and JP2 in extracts of young and adult hearts (20 μg per lane), using Caveolin 3 as the internal control on cardiac muscle ($N = 3–6$ mice

per group; see full blots in Supplementary Fig. 4) Data are shown as mean \pm standard error of the mean (SEM). * $P < 0.05$ between indicated groups based on Tukey–Kramer test. **g** Representative double staining of phalloidin (red) and DAPI (blue). Scale bar, 100 μm (upper panels). Representative electron micrographs of myofilaments in Floxed-TRPV2 and MCM-TRPV2-cKO hearts. Scale bar, 2 μm (lower panels).

TRPV2-deficient mice displayed changes in intercalated disc structure

We previously showed that cardiac TRPV2 localises to intercalated discs, and elimination of TRPV2 from adult mice leads to disorganisation of the intercalated disc structure and a decline in integrated cardiac pumping function¹⁸. The intercalated discs of adult Floxed-TRPV2 hearts exhibited a characteristic accordion structure, which was partially formed even in young hearts (Fig. 4a, upper panels). By contrast, the intercalated discs of adult MCM-TRPV2-cKO hearts showed extensive interdigitation and irregular shapes (Fig. 4a, lower right), and in young MCM-TRPV2-cKO hearts, the cell–cell contact sites were broad and loose, with no characteristic accordion structure (Fig. 4a, lower left). Furthermore, the gap junction protein Connexin 43 showed diffuse localisation in adult MCM-TRPV2-cKO hearts (Fig. 4a, lower panel). These results suggest that TRPV2 regulates the development of the intercalated disc structure.

The PI3K/Akt signalling pathway was downregulated in TRPV2-deficient hearts

To elucidate the molecular mechanism by which TRPV2 elimination from young mouse hearts impairs cardiac maturation, we analysed intracellular signalling in young and adult Floxed-TRPV2 and MCM-TRPV2-cKO mouse hearts. IGF-1 regulates cardiomyocyte maturation through IGF1R, a receptor tyrosine kinase that signals through the PI3K/AKT pathway¹. Compared with young Floxed-TRPV2 hearts, young MCM-TRPV2-cKO hearts displayed reduced IGF1R, PI3K, Akt, and S6K1 phosphorylation and mTOR expression (Fig. 5a–f), suggesting that the IGF1R pathway was downregulated and protein synthesis and mRNA expression were broadly suppressed, as evidenced by weak mTOR expression. IGF-1-induced cardiac hypertrophy is promoted by myocyte enhancer factor 2c (MEF2c), a key transcription factor complex involved in the differentiation and hypertrophic response of cardiomyocytes²⁴. MEF2c expression was lower in young MCM-TRPV2-cKO hearts than in young Floxed-TRPV2 hearts

(Fig. 5g), suggesting that gene expression essential for myocyte maturation was not promoted in the former. Phosphorylated Class II histone deacetylase (HDAC) associates with MEF2c and represses MEF2c activity²⁵. HDAC phosphorylation was suppressed in adult MCM-TRPV2-cKO hearts, indicating that MEF2c activity was not high even at that stage (Fig. 5h). SRF is one of the key regulators of cardiomyocyte maturation²⁶. In Floxed-TRPV2 mice, SRF expression was high in young hearts and low in adult hearts, whereas in MCM-TRPV2-cKO mice, SRF expression was low in both young hearts and adult hearts (Fig. 5i). IGF-1 expression, which promotes cardiac development and improves cardiac function²⁷, was also low in adult MCM-TRPV2-cKO hearts (Fig. 5j), likely because of reduced SRF expression. Overall, these results show that SRF-mediated transcription and IGF1R signalling were reduced in MCM-TRPV2-cKO hearts.

Maturation of Ca^{2+} handling and the MEF2c/HDAC axis were impaired in TRPV2-deficient cultured neonatal cardiomyocytes

In a previous study, we tracked the increase in cell area, reorganisation of myofibrils, and maturation of intracellular Ca^{2+} handling until the acquisition of synchronous beating in cultured neonatal cardiomyocytes¹⁸. To examine the role of TRPV2 in cardiomyocyte maturation, we used the same culture system to analyse intracellular Ca^{2+} handling and HDAC9 and MEF2c localisation in cardiomyocytes isolated from Floxed-TRPV2 or MCM-TRPV2-cKO neonatal mice. After 24 h of culture, Floxed-TRPV2 cardiomyocytes showed TRPV2 expression at the plasma membrane (Fig. 6a, upper left panel) and displayed ladder-like myofibers (Fig. 6a, upper right panel), indicating that sarcomere formation was in progress. On the other hand, MCM-TRPV2-cKO cardiomyocytes showed markedly attenuated TRPV2 expression and contained almost no myofibrils (Fig. 6a, lower panels), suggesting that TRPV2 is essential for myofibril maturation in cardiomyocytes.

We previously showed that mechanical stress from stretch or hypo-osmotic stimulation activates TRPV2^{16,18}. Floxed-TRPV2 cardiomyocytes

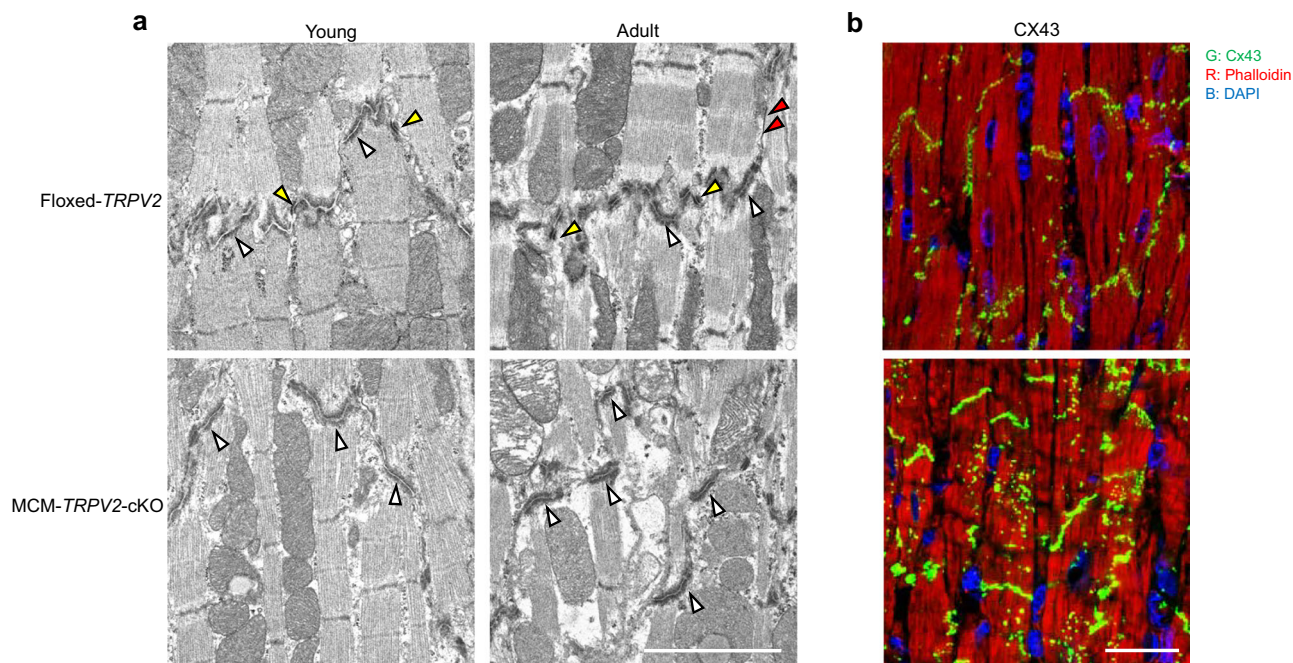


Fig. 4 | Abnormality of intercalated discs in MCM-TRPV2-cKO hearts. **a** Electron micrograph of intercalated discs in young and adult Floxed-TRPV2 and MCM-TRPV2-cKO mice. Scale bar, 1 μm. White triangles are adherence junctions. Yellow

triangles are desmosomes. Red triangles are gap junctions. **b** Triple staining of anti-Connexin 43 antibody (green), phalloidin (red), and DAPI (blue). Scale bar, 10 μm.

showed increased intracellular Ca^{2+} levels in response to hypo-osmotic stimulation. This response was blocked by addition of the TRPV2 inhibitor tranilast or by elimination of TRPV2, suggesting that TRPV2 was functional in the early phase of the culture process (Fig. 6b). Floxed-TRPV2 cardiomyocytes exhibited electrical stimulation-dependent Ca^{2+} transients and caffeine-induced Ca^{2+} release from the SR that became more pronounced over 72 h of culture (Fig. 6c, left panels). These cells also showed synchronised beating after 72 h in culture. In contrast, MCM-TRPV2-cKO cardiomyocytes showed no electrical stimulation-dependent Ca^{2+} response, no increase in Ca^{2+} content of the SR, and no synchronised beating after 72 h of culture (Fig. 6c, right panels, and 6d). These results indicate that the development of Ca^{2+} handling, which is essential for cardiomyocyte maturation, is dependent on TRPV2.

Ca^{2+} signalling in cardiomyocytes affects the function of transcription factors required for muscle maturation¹. In cultured cardiomyocytes, foetal calf serum (FCS) induces maturation with physiological hypertrophy. When Floxed-TRPV2 cardiomyocytes were cultured in FCS-containing medium, myofibers developed after 48 h (Fig. 6e, left panels). In these cells, HDAC9 and MEF2c localised in the intranuclear and intracellular spaces, respectively, in the absence of FCS and vice versa in the presence of FCS (Fig. 6e, left panels). On the other hand, HDAC9 and MEF2c had lower expression in MCM-TRPV2-cKO neonatal cardiomyocytes and did not change their localisation depending on the presence or absence of FCS in the culture medium (Fig. 6e, right panels). It was also clear that the myofibrils of the MCM-TRPV2-cKO cells were more fragile and weaker than those of the Floxed-TRPV2 cells (Fig. 6e, second panels from right). Forced expression of TRPV2 from an adenovirus in Floxed-TRPV2 cardiomyocytes resulted in nuclear localisation of MEF2c regardless of the presence of FCS (Fig. 6f). These results suggest that TRPV2 regulates the MEF2c/HDAC axis by enhancing Ca^{2+} handling during cardiomyocyte maturation.

IGF-1 treatment partially improves cardiac morphology and function in TRPV2-deficient mice

Cardiomyocytes secrete IGF-1 when stimulated with cyclic stretching²⁸. We previously showed that this cyclic stretch-dependent IGF-1 secretion is suppressed in TRPV2-deficient myocytes¹⁸. We used an adenovirus

construct, (Ad)-TRPV2, to increase TRPV2 expression in cultured cardiomyocytes from Floxed-TRPV2 mice, and we suppressed TRPV2 expression using Ad-Cre-recombinase with the LoxP system (Fig. 7a, b; Supplementary Fig. 2). Ad-TRPV2 markedly upregulated IGF-1 expression in cultured cardiomyocytes, whereas Ad-Cre downregulated IGF-1 expression, confirming that TRPV2 controls IGF-1 expression (Fig. 7a, c). Notably, Ad-Cre also suppressed myofiber formation (Fig. 7a, c). To determine whether IGF-1 treatment can enhance cardiac growth and function in mice with TRPV2 deficiency from early childhood, we continuously administered IGF-1 to Floxed-TRPV2 and MCM-TRPV2-cKO mice starting at 3 weeks of age and examined cardiac function and cardiomyocyte morphology at 12 weeks of age. Continuous administration of IGF-1 increased cardiac size and function in MCM-TRPV2-cKO mice, although these mice did not show the same cardiac hypertrophy as Floxed-TRPV2 mice (Fig. 7d–i). In addition, IGF-1 administration almost restored the ladder-like myofilament structure and normal localisation of Ca^{2+} regulators in MCM-TRPV2-cKO hearts (Fig. 7j, lower panels). These results indicate that the IGF-1 pathway is partially involved in the process by which TRPV2 promotes the maturation of cardiac structure and function.

TRPV2-deficient mice had an impaired response to dobutamine stress challenge

To evaluate the stress response in TRPV2-deficient hearts, we treated adult Floxed-TRPV2 and MCM-TRPV2-cKO mice with 5 mg/kg dobutamine, a sympathomimetic drug that stimulates adrenergic receptors to increase heart rate and contractility²⁹. As expected, heart rate increased in Floxed-TRPV2 mice and MCM-TRPV2-cKO mice 4 min after dobutamine injection (percent increase over baseline heart rate: Floxed-TRPV2, 19.06% ± 2.15% vs. MCM-TRPV2-cKO, 21.21% ± 4.57%; $P = 0.685$; Fig. 8a). In terms of heart contractility (as indicated by FS%), Floxed-TRPV2 mice showed a marked increase after dobutamine treatment, whereas MCM-TRPV2-cKO mice showed little change (percent increase over baseline FS%: Floxed-TRPV2, 22.08% ± 1.13% vs. MCM-TRPV2-cKO, 1.89% ± 2.47%; $P < 0.0001$), likely due to decreased contractile reserve, which is common in heart failure³⁰ (Fig. 8b–e). These results suggest that cardiac TRPV2 is essential for the development of stress tolerance.

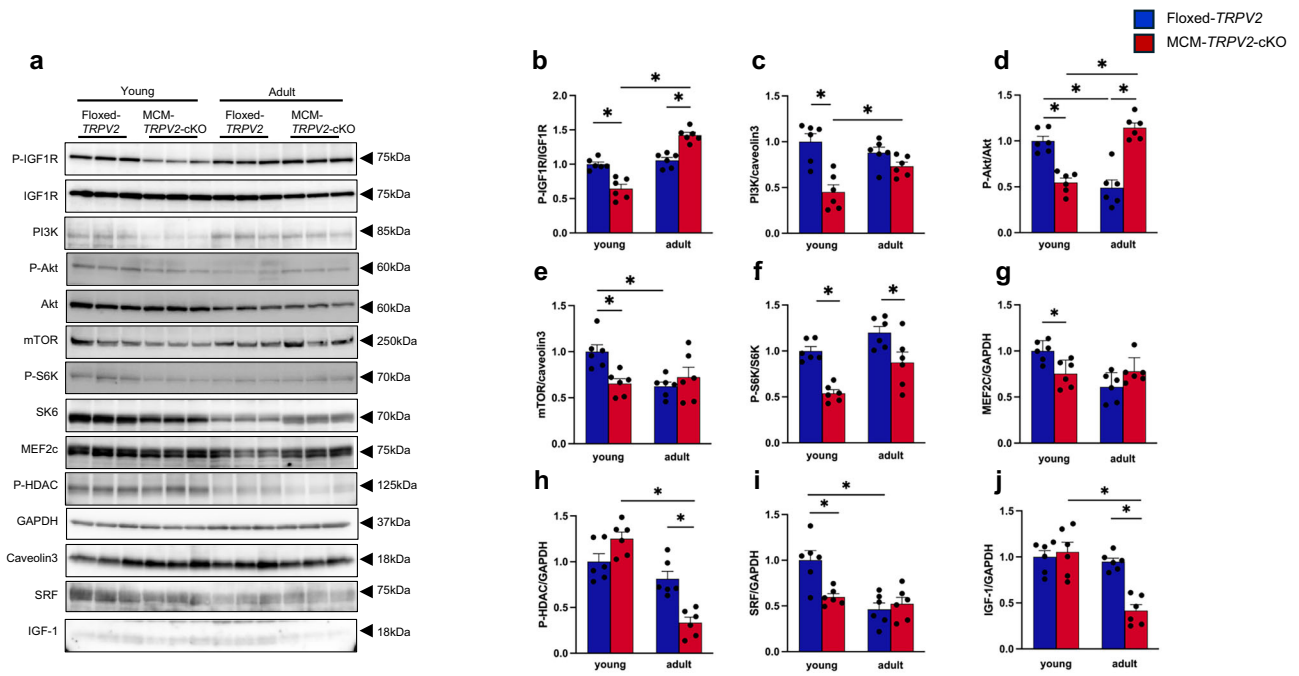


Fig. 5 | Changes in expression of IGF-1, MEF2c, HDAC, and SRF in MCM-TRPV2-cKO hearts. a Representative immunoblots of young and adult Floxed-TRPV2 and MCM-TRPV2-cKO hearts. (*N* = 6 mice per group; see full blots in

Supplementary Fig. 4) b–j Data summarising the expression levels of each molecule. Data are shown as mean ± standard error of the mean (SEM). **P* < 0.05 between indicated groups based on Tukey–Kramer test.

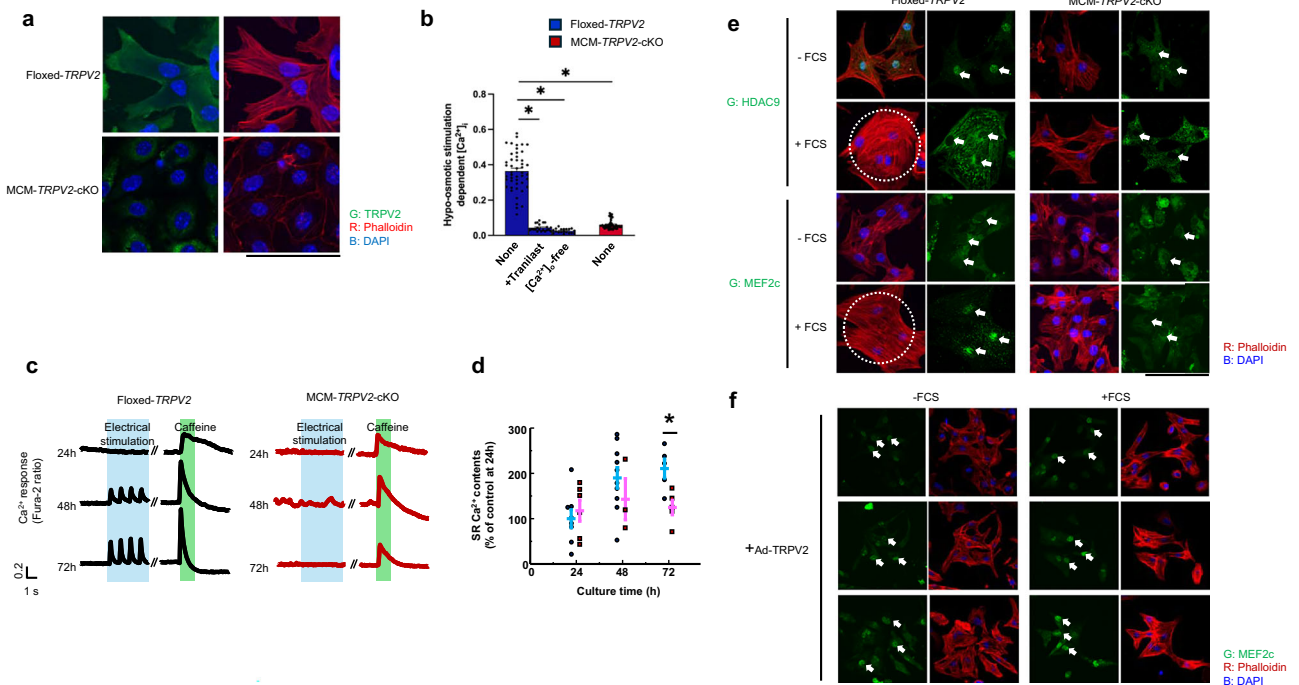


Fig. 6 | Impaired actin organisation, Ca²⁺ handling, and MEF2c/HDAC axis in cultured cardiomyocytes isolated from MCM-TRPV2-cKO hearts. a Triple staining of anti-TRPV2 (green), phalloidin (red), and DAPI (blue). Scale bar, 50 μm b Hypo-osmotic stimulation-dependent intracellular Ca²⁺ increase in Floxed-TRPV2 and MCM-TRPV2-cKO cardiomyocytes (*n* = 19–47 cells from three hearts per group). Data are shown as mean ± standard error of the mean (SEM). **P* < 0.05 vs. cells from other groups based on Tukey–Kramer test. c Representative electrical stimulation- and caffeine-induced Ca²⁺ response in Floxed-TRPV2 and MCM-TRPV2-cKO cardiomyocytes. d Estimation of

sarcoplasmic reticulum (SR) Ca²⁺ content (*n* = 3–10 cells from three hearts per group). Data are shown as mean ± standard error of the mean (SEM). **P* < 0.05 vs. Floxed-TRPV2 mice at the same frequency based on Student’s *t*-test. e Localisation of HDAC9 and MEF2c (green) in Floxed-TRPV2 and MCM-TRPV2-cKO cardiomyocytes. Red and blue indicate phalloidin and DAPI, respectively. White arrows indicate nuclear location. Actin development is seen within the dotted circles. Scale bar, 50 μm. f Localisation of MEF2c (green) in Floxed-TRPV2 cardiomyocytes infected with Ad-TRPV2. White arrows indicate nuclear location. Scale bar, 50 μm.

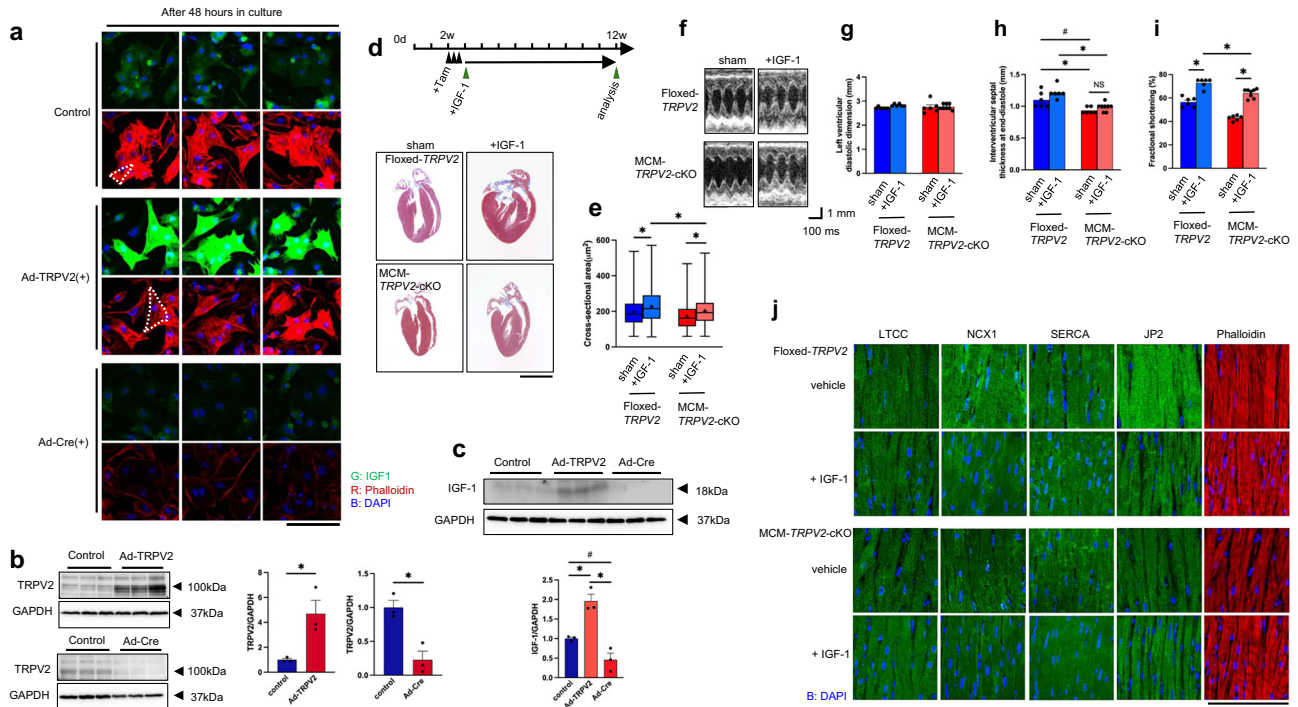


Fig. 7 | TRPV2 dependence of IGF-1 expression and partial recovery of cardiac structure and function by IGF-1 administration. **a** Changes in IGF-1 expression and actin formation dependent on TRPV2 expression. Representative immunostaining for IGF-1 (green), phalloidin (red), and DAPI (blue). Scale bar, 200 μ m. **b** Expression of TRPV2 protein in Ad-TRPV2-infected myocytes (upper panels) or Ad-Cre-infected myocytes (lower panels). **c** Expression of IGF-1 protein in Ad-TRPV2- or Ad-Cre-infected myocytes ($N = 3$ mice per group). $*P < 0.05$ vs. hearts from other groups based on Tukey–Kramer test. **d** Schedule of IGF-1 administration after 8 weeks of IGF-1 administration. Scale bar, 5 mm. **e** Cross-sectional area from paraffin sections of left ventricles ($n = 518$ –2480 cells from 3 mice per group). Centre line = median; + = mean; box limits = upper

and lower quartiles, whiskers = minimum and maximum. **f** Representative tracing of two-dimensional transthoracic M-mode echocardiography. **g–i** Echocardiographic assessment of left ventricular diastolic dimension, interventricular septal thickness at end-diastole, and fractional shortening ($N = 6$ –8 mice per group). $*P < 0.05$ vs. multiple comparisons based on Tukey–Kramer test. # $P < 0.05$ vs. sham-operated Floxed-TRPV2 based on Student’s t -test. **j** Change in localisation of LTCC, NCX1, SERCA, JP2, and myofilament structure in Floxed-TRPV2 and MCM-TRPV2-cKO hearts. Double staining of the antibody of target protein (Green) or phalloidin (red) and DAPI (blue). Scale bar, 100 μ m. Data are shown as mean \pm standard error of the mean (SEM).

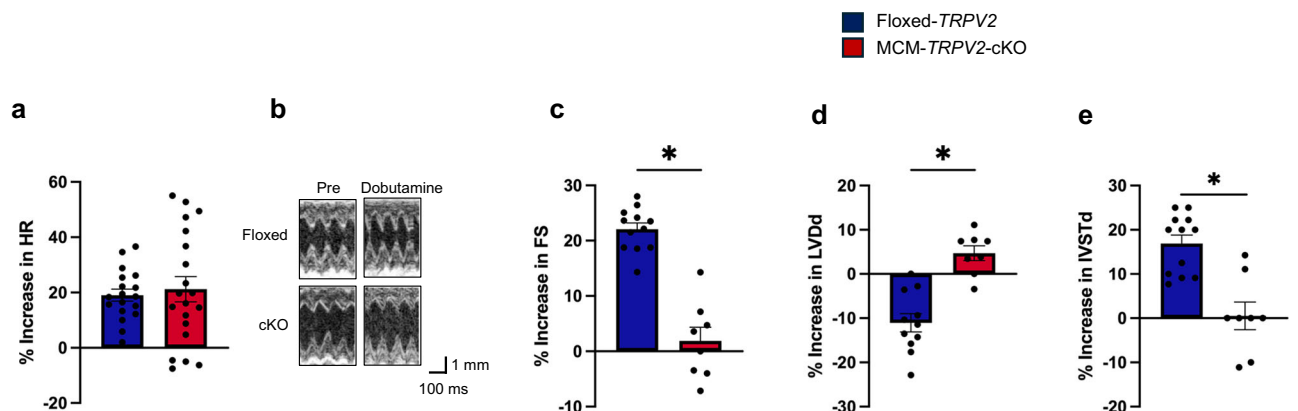


Fig. 8 | Dobutamine stress challenge in Floxed-TRPV2 and MCM-TRPV2-cKO mice. **a** Change in heart rate ($N = 18$ –20 mice per group). **b** Representative tracing of two-dimensional transthoracic M-mode echocardiography. **c–e** Echocardiographic assessment of fractional shortening, left ventricular diastolic

dimension, and interventricular septal thickness at end-diastole ($N = 8$ –12 mice per group). Data are shown as mean \pm standard error of the mean (SEM). $*P < 0.05$ vs. Floxed-TRPV2 mice based on Student’s t -test.

TRPV2-deficient mice had an impaired hypertrophic response

To clarify the effect of TRPV2 deficiency under conditions of chronic haemodynamic stress, we treated Floxed-TRPV2 and MCM-TRPV2-cKO mice with the adrenergic receptor agonist phenylephrine (PE) to induce hypertrophy and pathological remodelling. After 2 weeks of PE administration, Floxed-TRPV2 mice showed an adaptive hypertrophic

response with increased heart-to-body-weight ratio and no chamber dilation or cardiac dysfunction, whereas MCM-TRPV2-cKO mice showed chamber enlargement with fibrosis and severe cardiac dysfunction without any increase in heart-to-body-weight ratio or cell area (Fig. 9a–h). To elucidate the mechanism of stress-dependent responses in MCM-TRPV2-cKO hearts, we analysed Akt phosphorylation and the

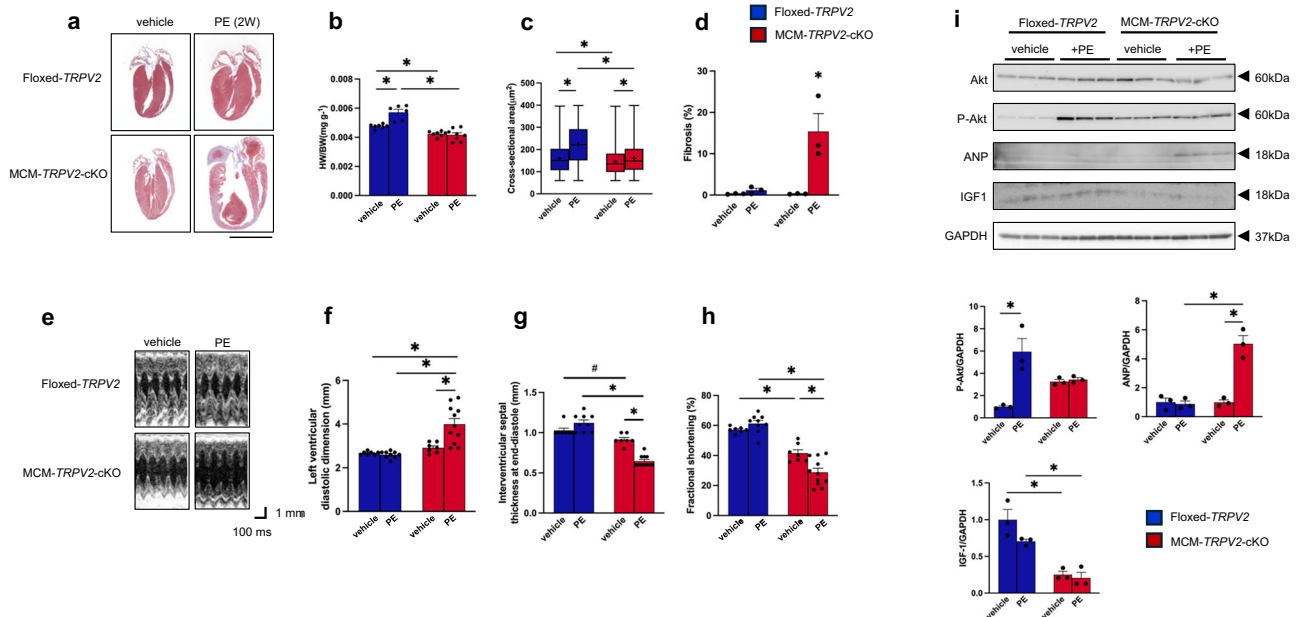


Fig. 9 | Changes induced by PE administration in MCM-TRPV2-cKO mice. **a** Histological analysis after 2 weeks of PE administration. Scale bar, 5 mm. **b** Changes in heart-to-body weight (HW/BW) ratio ($N = 6-8$ mice per group). **c** Changes in cross-sectional area of cardiomyocytes ($n = 1110-2060$ cells from 3 mice per group). Centre line = median; + = mean; box limits = upper and lower quartiles, whiskers = minimum and maximum. **d** Fibrosis percentage ($N = 3$ hearts per group). **e** Representative tracing of two-dimensional transthoracic M-mode

echocardiography. **f-h** Echocardiographic assessment of left ventricular diastolic dimension, interventricular septal thickness at end-diastole, and fractional shortening ($N = 7-11$ mice per group). * $P < 0.05$ vs. multiple comparisons based on Tukey-Kramer test. # $P < 0.05$ vs. vehicle-treated Floxed-TRPV2 based on Student's *t*-test. **i** Representative immunoblots. ($N = 3$ mice) * $P < 0.05$ vs. multiple comparisons based on Tukey-Kramer test. Data are shown as mean \pm standard error of the mean (SEM).

expression of IGF-1 and atrial natriuretic peptide (ANP), a marker of elevated preload and cardiac dysfunction. Floxed-TRPV2 hearts showed increased AKT phosphorylation but no increase in ANP expression after PE administration, whereas MCM-TRPV2-cKO hearts showed increased ANP expression but no change in AKT phosphorylation, suggesting that PE treatment was more stressful for MCM-TRPV2-cKO hearts than for Floxed-TRPV2 hearts (Fig. 9i). IGF-1 expression was always lower in MCM-TRPV2-cKO hearts than in Floxed-TRPV2 hearts, with or without PE treatment (Fig. 9i). These results suggest that TRPV2 is required for the development of cardiomyocytes that can adaptively respond to haemodynamic stress.

Finally, we examined the effect of TRPV2 deficiency on cardiac pathological remodelling in response to a more direct mechanical stress, pressure overload. Floxed-TRPV2 hearts showed an adaptive hypertrophic response after 2 to 8 weeks of transverse aortic constriction (TAC; Fig. 10a, b) and developed heart failure with reduced cardiac function and ventricular dilation with fibrosis after 16 weeks (Fig. 10c-h). On the other hand, MCM-TRPV2-cKO hearts showed no significant morphological or functional changes after TAC (Fig. 10a-h), suggesting that they were unable to sense pressure overload. Akt and Rac1 phosphorylation and ANP and IGF-1 expression were elevated after TAC in Floxed-TRPV2 hearts, suggesting a mechanical stress-dependent hypertrophic response (Fig. 10i). By contrast, there was no post-TAC upregulation of these molecules in MCM-TRPV2-cKO hearts. Rac1 mediates the mechanotransduction pathway, and pressure overload induces Rac1 phosphorylation in the heart³¹. The phosphorylation level of Rac1 was reduced in MCM-TRPV2-cKO hearts subjected to pressure overload, reflecting a lack of mechanical stress sensing, even after TAC treatment (Fig. 10i). These results suggest that TRPV2 is involved in the mechanotransduction process of cardiomyocytes during hemodynamic stress. Taken together, the results show that hearts deficient in TRPV2 from an early age were unable to adaptively mount hypertrophic responses to PE administration or to TAC surgery and were significantly less resilient to stress.

Discussion

Haemodynamic stress is an important factor that promotes physiological growth and pathological hypertrophy^{1,4,20,32-34}; however, the molecular mechanism of its mechanotransduction in cardiomyocytes remains unclear. We previously showed that TRPV2 is required for cellular Ca^{2+} responses to stretch and hypo-osmotic stimuli¹⁶⁻¹⁸. In our previous study, TRPV2 elimination from adult mice resulted in severe heart failure within a few days and about 70% death within 10 days¹⁸. This suggests that TRPV2 is indispensable in the adult working heart. In the present study, TRPV2 was eliminated in the heart at 2 weeks of age, but the survival of the mice was unaffected, allowing analysis of the role of TRPV2 during growth. The difference in survival rates depending on the timing of TRPV2 elimination might be due to differences in the role of TRPV2 at different stages of cardiac development. In the case of TRPV2 elimination in the adult heart, disruption of intercalated discs led to structural and functional abnormalities of cardiomyocytes, which resulted in severe cardiac dysfunction due to a lack of electrical and mechanical coupling between cardiomyocytes¹⁸. In contrast, juvenile hearts were less affected by TRPV2 elimination because of their inherently weak cardiac contractility and immature intercalated disc structure; however, the TRPV2-deficient cardiomyocytes did not promote structural and functional maturation, remained weakly contractile, and lacked stress tolerance once the mice reached adulthood. This suggests that TRPV2 is crucial for the maturation of cardiomyocyte stress resilience.

We propose two hypotheses regarding the observed impairment of cardiac growth and function in mice that lack cardiac TRPV2 expression from a young age. First, decreased SRF-mediated transcription in the growing heart suppresses cardiomyocyte maturation. Overexpression of SRF in the mouse heart results in hypertrophic cardiomyopathy³⁵, and overproduction of a dominant-negative mutant form of SRF causes severe cardiac dilation and death³⁶. Temporary cardiomyocyte-specific SRF knockout does not result in hypertrophic compensation, despite compensatory increases in several other key factors³⁷. This suggests that SRF is an important mediator of both physiological growth and pathological hypertrophy. In addition, we found that continuous administration of IGF-1 from

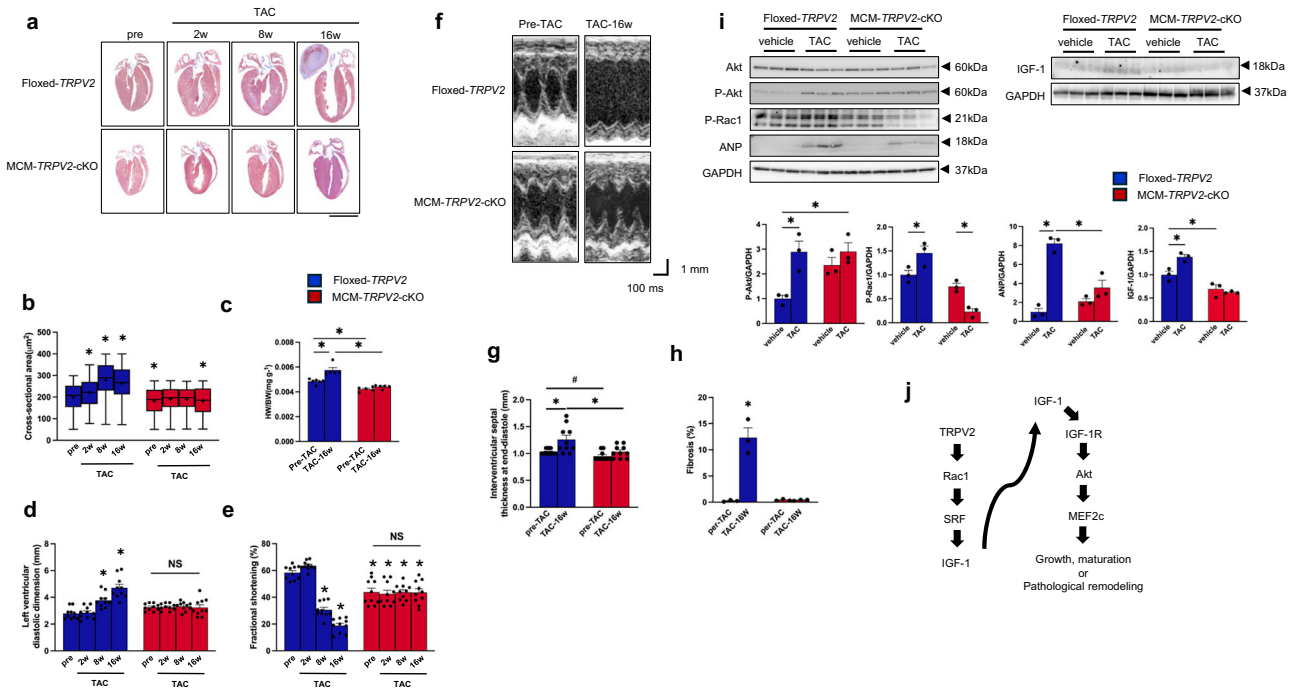


Fig. 10 | Changes induced by pressure overload in MCM-TRPV2-cKO mice. **a** Histological analysis 2, 8, and 16 weeks after pressure overload induction. Scale bar, 5 mm. **b** Changes in cross-sectional area of cardiomyocytes ($n = 144\text{--}504$ cells from 3 mice per group). Centre line = median; + = mean; box limits = upper and lower quartiles, whiskers = minimum and maximum. **c** Changes in heart-to-body weight (HW/BW) ratio ($N = 5\text{--}6$ mice per group). **d, e** Echocardiographic assessment of left ventricular end dimension at systole and fractional shortening ($N = 10$ mice per group). * $P < 0.05$ in multiple comparisons based on Tukey–Kramer test. **f** Representative tracing of two-dimensional transthoracic M-mode

echocardiography. **g** Echocardiographic assessment of interventricular septal thickness at end-diastole. * $P < 0.05$ in multiple comparisons based on Tukey–Kramer test. # $P < 0.05$ vs. pre-TAC Floxed-TRPV2 based on Student’s t -test. **h** Fibrosis percentage ($N = 3$ hearts per group). **i** Representative immunoblots of hearts treated with vehicle or TAC after 16 weeks. ($N = 3$ mice) * $P < 0.05$ vs. multiple comparisons based on Tukey–Kramer test. **j** Estimated TRPV2 signal pathway affecting maturation and pathological remodelling. Data are shown as mean \pm standard error of the mean (SEM).

youth in MCM-TRPV2-cKO mice did not result in hypertrophic correction (Fig. 7), which is consistent with the effects seen in SRF-deficient mice³⁷. Our experimental results suggest that cardiac TRPV2 promotes physiological growth and hypertrophy via activation of SRF-mediated transcription.

Second, abnormal intercalated discs and impaired cardiomyocyte contractility reduce cardiac integrity in TRPV2-deficient hearts, which leads to reduced sensing of biomechanical stress that is essential for normal cardiac functional and morphological maturation. The intercalated disc is a specialised structure at the connection between cardiomyocytes that are subjected to mechanical stress with each heartbeat and undergoes remodelling in various cardiac pathologies, including pressure overload^{38,39}. Sarcomere elongation is proposed to occur at intercalated discs in the growing heart, and changes at these sites play a major role in regulating cardiomyocyte size⁴⁰. The absence of accordion-like structures in the areas of cell–cell contact in MCM-TRPV2-cKO hearts might limit sarcomere elongation (Fig. 4a). The disrupted localisation of Connexin 43 also suggests that electrical coupling between neighbouring cardiomyocytes is impaired in MCM-TRPV2-cKO hearts (Fig. 4b). These disruptions of cardiac integrity reduce mechanical feedback to the cardiomyocytes, retarding their growth.

Young TRPV2-deficient hearts showed dramatically reduced SERCA2a expression (Fig. 3b, f). Because cardiomyocyte contractility is low in the young stage, with or without TRPV2 (Fig. 2a, b), reduced SERCA2a expression (Fig. 3b) would not affect cardiomyocyte physiology in young MCM-TRPV2-cKO mice. It might, however, affect the intracellular Ca^{2+} homeostasis of cardiomyocytes. The attenuated IGF1R/PI3K/Akt pathway, which is regulated by intracellular Ca^{2+} in young TRPV2-cKO hearts, also suggests that Ca^{2+} homeostasis is disordered in cKO myocytes.

Mice with cardiac-specific SERCA2a knockout exhibit impaired cardiac function due to disruption of cardiomyocyte contractility, Ca^{2+}

handling, and energy metabolism^{41–43}. Loss of SERCA2a leads not only to SR collapse but also to remodelling of the T-tubule so that the intracellular dyad structure is disorganised⁴⁴. In our study of adult TRPV2-deficient hearts, the localisation of LTCC and NCX, which are originally located in the T-tubule, is disrupted, and the localisation of SERCA2a and JP2 is also abnormal (Fig. 3a). Therefore, downregulation of SERCA2a at a young age appears to influence the formation of the T-tubule and dyad structure during growth in MCM-TRPV2-cKO hearts.

The increased expression of SERCA2a in MCM-TRPV2-cKO adult hearts might be a response to compensate for reduced SR function (Fig. 3b, f); however, the Ca^{2+} handling and SR Ca^{2+} content of isolated cells were reduced in MCM-TRPV2-cKO adult hearts (Fig. 2d–g). This is probably because Ca^{2+} handling and SR function for efficient E-C coupling cannot be maintained if the structure of T-tubules and dyads is disrupted, even if SERCA2a expression levels are high. This is consistent with our previous findings¹⁸. Elimination of TRPV2 from adult mouse hearts resulted in breakdown of T-tubule and dyad structure and impaired Ca^{2+} handling and SR function associated with E-C coupling, although Ca^{2+} transporter and SERCA expression was unchanged¹⁸. Therefore, during cardiac growth, TRPV2 appears to regulate signals involved in the formation of T-tubules and dyad structure, although the molecular mechanisms need to be clarified.

IGF-1 is produced mainly in the liver, and the circulating level of IGF-1 increases soon after birth under the influence of growth hormone^{45,46}. IGF-1 continues to be secreted throughout life under normal conditions and in response to changes in intracellular Ca^{2+} concentration due to mechanical stress^{47–49}. This mechanoresponsive IGF-1 secretion, in turn, modulates the myocyte IGF1R/PI3K/Akt pathway, which is involved in myocardial hypertrophy and heart failure⁴⁷. In MCM-TRPV2-cKO hearts, the expression levels of IGF-1 and its upstream regulator SRF were consistently low

regardless of haemodynamic stress (Figs. 5i, j, 9i and 10i), suggesting that TRPV2 signalling controls IGF-1 expression. In support of this idea, we found that forced expression of TRPV2 in cultured cardiomyocytes markedly increased cell area and IGF-1 expression (Fig. 7a, c) and enhanced MEF2c nuclear translocation (Fig. 6f). In addition, MCM-TRPV2-cKO hearts had an attenuated IGF1R/PI3K/Akt pathway from a young age (Fig. 5), consistent with previous results in adult mice with acute TRPV2 elimination¹⁸. These results suggest that TRPV2 signalling regulates cardiomyocyte maturation via the IGF-1 signalling pathway, although the mechanism remains to be uncovered.

Increased contractility during growth enhances cardiomyocyte maturation through mechanical feedback^{34,50}. The TRPV2-dependent myofiber formation observed in this study (Figs. 3g and 6a) provides positive mechanical feedback to cardiomyocytes within the working heart, leading to cardiomyocyte maturation. We showed that TRPV2 is involved in the mechanical stress-dependent Ca²⁺ response of cardiomyocytes (Fig. 6b), although it remains unclear whether TRPV2 directly senses mechanical stress. In immature cardiomyocytes, Ca²⁺ influx from the extracellular space during heartbeat contributes to the formation of Ca²⁺ transients for contraction and Ca²⁺ signalling⁵¹. TRPV2 might be involved in this pathway and contribute to cardiomyocyte maturation as an important extracellular Ca²⁺ supplier that functions with increased contractility. This idea is supported by the fact that TRPV2-deficient cells showed no increases in Ca²⁺ transients involved in E-C coupling or SR Ca²⁺ content during culture (Fig. 6c, d). Hence, the promotion of TRPV2 activity in immature cardiomyocytes might be an effective strategy to induce maturation and differentiation for developmental engineering and regenerative medicine.

TRPV2 is widely expressed throughout the body^{16,17,52,53}. Mice with systemic TRPV2 deficiency were susceptible to perinatal lethality⁵⁴, suggesting that TRPV2 is crucial for foetal survival and development. Recently, TRPV2-based therapies have begun to attract attention in the field of cardiovascular medicine⁵⁵, and the specific roles of TRPV2 in different tissues, stages of growth and development, and pathologies need to be clarified. This study provides a detailed analysis of the importance of TRPV2 in cardiac growth, cardiomyocyte maturation, and pathological remodelling. The integrated performance of the circulatory system can be discussed for the treatment of cardiovascular pathologies by comparing our findings with previous findings from mice with systemic TRPV2 deficiency^{19,56}. In addition, the detailed roles of TRPV2 in blood vessels and muscle should be analysed using mice with other tissue-specific TRPV2 knockouts in future work.

Several studies have raised concerns that tamoxifen treatment can adversely influence cardiac function in adult MCM mice^{57,58}. A DNA damage response occurs in these hearts, resulting in cardiomyocyte apoptosis, cardiac fibrosis, and cardiac dysfunction⁵⁷. Therefore, Koitabashi et al.⁵⁸ recommended a reduced tamoxifen dosage of <20 mg/kg body weight per day for use in MCM^{+/-} mice (an approximate total dose of 80 mg/kg). In previous studies^{18,21}, we administered tamoxifen by intraperitoneal (i.p.) injection consecutively for 4 days at a dose of 8 mg/kg body weight in 10-week-old MCM^{+/-} mice (8 mg/kg per day, approximate total dose of 32 mg/kg). In a microarray analysis, we were unable to detect any alterations in the signalling pathways involved in DNA damage response in MCM^{+/-} hearts treated with tamoxifen for 4 days²¹. In the same previous studies, we found that TRPV2 mRNA was suppressed by more than 95% on day 3 after tamoxifen administration¹⁸. Therefore, in the present study, the duration of tamoxifen administration was shortened to 3 days with the aim of decreasing tamoxifen use. The fact that TRPV2 protein expression was suppressed by more than 95% with this protocol is confirmed in Fig. 1b. In addition, tamoxifen treatment did not affect overall cardiac structure and function in TRPV2^{fllox/+}; MCM^{+/-} (hetero) mice (Supplementary Fig. 3). Together, our results indicate that the heart-failure phenotype seen in tamoxifen-treated MCM-TRPV2-cKO mice was not due to adverse effects of tamoxifen or excessive MCM expression.

Methods

Animal experiments

We have complied with all relevant ethical regulations for animal. The Institutional Animal Care and Use Committee at Okayama University and KINJO GAKUIN University approved the animal experiments conducted in this study (approval number OKU-2022397, 2021119 in Okayama University; 249, 272 in KINJO GAKUIN University). All methods were carried out in accordance with the Guide for the Care and Use of Laboratory Animals published by the U.S. National Institutes of Health.

Animals

The generation of TRPV2^{fllox/fllox};MerCreMer^{+/-} (MCM-TRPV2-cKO) and TRPV2^{fllox/fllox};MerCreMer^{-/-} (Floxed-TRPV2) mice was previously described in detail (Katanosaka et al., 2014, Nat. Comms.). To induce Cre-mediated recombination, 2-week-old MCM-TRPV2-cKO and Floxed-TRPV2 mice were injected intraperitoneally (i.p.) with 8 mg/kg tamoxifen (Sigma) once daily for 3 consecutive days. Littermates were used in this study to randomise genetic variation. To examine the hypertrophic response, mice were implanted subcutaneously with osmotic infusion pumps, and 40 mg/kg phenylephrine (PE) was administered.

TAC surgery

TAC surgery was performed to induce left ventricular pressure overload. The detailed methods have been described previously (Ujihara, Y. et al., 2016, Cardiovasc. Res.). Male mice (10 weeks old) were anaesthetised with the combination anaesthetic consisting of 0.3 mg/kg medetomidine (Zenoaq), 4.0 mg/kg midazolam (Sandoz), and 5.0 mg/kg butorphanol (Meiji Seika Pharma). After orotracheal intubation, a cannula was connected to a volume-cycled ventilator (SN-480-7; Shimano) using room air at a tidal volume of 0.2 ml and a respiratory rate of 110 breaths/min. A small incision through the second intercostal space was made to access the chest cavity, and the transverse aorta was constricted with a 7-0 nylon string by ligation with a blunted 27-gauge needle, which was later removed.

Administration of IGF-1

IGF-1 administration and tamoxifen treatment were started at the same time from 2 weeks of age. Control mice received vehicle alone. Recombinant human IGF-1 was purchased from Cell Science, diluted with 0.9% NaCl at a concentration of 10 mg/mL, and intraperitoneally injected to mice (50 µg per day) from 2 to 4 weeks of age. Thereafter, recombinant IGF-1 was administered to mice (60 µg per day) by continuous infusion (0.25 µL per h) using a mini osmotic pump (Alzet 1004).

Neonatal cardiomyocyte culture

Primary cardiomyocyte cultures were prepared from ventricles of 1-day-old mice by very gentle trypsinisation at room temperature using a modified method for rat neonatal hearts⁵⁹. Briefly, neonatal MCM-TRPV2-cKO or control (floxed) mice were anaesthetised by inhalation of isoflurane, and their hearts were rapidly removed. The ventricles were excised, cut into several pieces, and washed three times with 10 mL ice-cold phosphate-buffered saline (PBS) for 1 min by gentle shaking. The tissue pieces were digested three times with 0.06% trypsin in Dulbecco's modified eagle medium (DMEM) (8 mL) for 8 min at 37 °C by gentle agitation. The cells were resuspended in DMEM with 10% FCS to stop trypsinisation and centrifuged at 1400×g for 3 min. The cell pellets were resuspended in fresh DMEM containing 10% FCS, plated on collagen-coated 24-well dishes at a density of 4 × 10⁴ cells per well, and maintained in DMEM containing 10% FCS and 2 µg/mL 4-hydroxy tamoxifen (sigma). In some experiments, after confirming cell adhesion, the cells were infected with adenovirus for 24 h.

Isolation of adult mouse ventricular myocytes

Ventricular myocytes were obtained from 10-week-old male mice using a method previously described^{18,20,21}. Adult mice were anaesthetised by isoflurane inhalation and euthanised with pentobarbital (50 mg/kg, i.p.), and their hearts were rapidly removed and Langendorff-perfused at a constant

hydrostatic pressure of 70-cm H₂O at 37 °C using cell-isolation buffer (CIB) supplemented with 0.4 mM EGTA (EGTA-CIB), which chelates calcium within the heart. CIB contained 130 mM NaCl, 5.4 mM KCl, 0.5 mM MgCl₂, 0.33 mM NaH₂PO₄, 22 mM glucose, 50 nM/mL bovine insulin (Sigma), and 25 HEPES-NaOH (pH = 7.4). Bovine insulin was used from 1 U/mL stock solution in 0.1 mM HCl (pH = 4.0), and EGTA was used from a 400 mM stock in 1 M NaOH (pH = 7.8). The perfusate was then switched to the enzyme solution (15 mL), which consisted of CIB supplemented with 0.3 mM CaCl₂, 1 mg/mL collagenase (Worthington Biochemical), 0.06 mg/mL trypsin (Sigma), and 0.06 mg/mL protease (Sigma). Once the tissue had undergone complete digestion, the ventricles were excised, cut into several pieces, and further digested in fresh enzyme solution (15 mL) for 15–20 min at 37 °C until they were mostly dissociated. In this enzyme solution, the CaCl₂ level was increased to 0.7 mM, and 2 mg/mL BSA (Sigma) was supplemented. The cell suspension was centrifuged at 14×g for 3 min. The cell pellet (~0.1 ml) was resuspended in CIB supplemented with 1.2 mM CaCl₂ and 2 mg/mL BSA, incubated at 37 °C for 10 min, centrifuged (14×g, 3 min), and resuspended in 10 mL Tyrode's solution supplemented with 2 mg/mL BSA. Tyrode's solution contained 140 mM NaCl, 5.4 mM KCl, 1.8 mM CaCl₂, 0.5 mM MgCl₂, 0.33 mM NaH₂PO₄, 11 mM glucose, and 5 mM HEPES-NaOH (pH = 7.4).

Measurement of cell shortening and intracellular Ca²⁺ transients in adult cardiac myocytes

We examined cell shortening and Ca²⁺ transients in isolated cardiomyocytes after loading with 10 μmol/L Indo-1 AM (Invitrogen) and electrical stimulation at a frequency of 1 Hz using a two-platinum electrode insert connected to a bipolar stimulator (SEN-3301; Nihon Kohden) on the stage of an inverted microscope (IX71; Olympus) with a 20× water immersion objective lens (UApo N340; Olympus). Ca²⁺ transients were evaluated as the fluorescence ratio at 405:480 nm, emitted by cells upon excitation at 340 nm, using a high-performance Evolve™ EMCCD camera (Photometrics). Cardiomyocytes were maintained under a continuous flow of standard Tyrode's solution using a microperfusion system. Ca²⁺ transients were recorded and analysed using MetaMorph version 7.7.1.0 software (Molecular Devices Inc.). Means of the fluorescent signals from 10–20 cardiomyocytes from a single heart were calculated. The standard deviation of the normalised value at the peak was taken as a measure of the synchrony of Ca²⁺ release.

Measurement of intracellular Ca²⁺ in newborn cardiomyocytes

Intracellular Ca²⁺ change was examined in cardiomyocytes loaded with 2 μM fura-2-acetoxymethyl ester (fura-2) for 30 min at 37 °C and maintained in standard Tyrode's solution under continuous flow using a microperfusion system. Fura-2-loaded cells were alternately excited at 340 nm and 380 nm using a Lambda DG-4 Ultra High Speed Wavelength Switcher (Sutter Instruments) coupled to an inverted IX71 microscope with a UApo 20×/0.75 objective lens (Olympus). Fura-2 fluorescent signals were recorded (ORCA-Flash 2.8; Hamamatsu Photonics) and analysed by a ratiometric fluorescence method using MetaFluor software (version 7.7.5.0; Molecular Devices).

Antibodies

The following antibodies were used for immunostaining and immunoblot analysis: anti-LTCC (Alomone, 1:1000 dilution), anti-SERCA2a (Thermo, 1:1000 dilution), anti-GAPDH (Abcam, 1:1000 dilution), anti-caveolin3 (BD biosciences, 1:1000 dilution), anti-junctophilin2 (Santa Cruz, 1:1000 dilution), anti-IGF-1 receptor (Cell Signaling, 1:1000 dilution), anti-phospho-IGF-1 receptor (Cell Signaling, 1:1000 dilution), anti-Akt (Cell Signaling, 1:1000 dilution), anti-phospho-Akt (Cell Signaling, 1:1000 dilution), anti-mTOR (Cell Signaling, 1:1000 dilution), anti-PI3K (Cell Signaling, 1:1000 dilution), anti-p70S6K (Cell Signaling, 1:1000 dilution), anti-phospho-p70S6K (Cell Signaling, 1:1000 dilution), anti-MEF2C (Cell Signaling, 1:1000 dilution), anti-p-HDAC (Sigma, 1:1000 dilution), anti-IGF-1 (Santa Cruz, 1:1000 dilution), and anti-SRF (Santa Cruz, 1:1000 dilution). Anti-NCX1 antibody (1:1000 dilution) was generated in our laboratory as previously described (Katanosaka et al., 2005, J Bio Chem).

Immunoreactive bands were visualised using an enhanced chemiluminescence detection system (Amersham Biosciences Corp.) and a Luminescent Image Analyzer (LAS3000; Fujifilm).

Histological analysis

Hearts were excised, fixed immediately in buffered 4% paraformaldehyde, embedded in paraffin, and cut into 4-μm sections. For electron microscopy, hearts were fixed in 2% paraformaldehyde and 2% glutaraldehyde in PBS. Samples were stained with Masson's trichrome or processed for immunohistochemistry.

Electron microscopy

For electron microscopy, excised hearts were fixed in 2% paraformaldehyde and 2% glutaraldehyde in PBS. The sections were examined under a JEM-1200 electron microscope (Nihondensi, Co., Japan).

Preparation of heart extracts and immunoblotting

Mouse hearts were homogenised using a Hiscotron homogeniser (NITI-ON) in RIPA buffer. Lysates were centrifuged at 100,000×g for 20 min. The supernatant was analysed by immunoblotting as previously described (Katanosaka et al., 2014, Nat. Comms.).

Statistics and reproducibility

Experimenters who collected or quantified data were blinded to genotype, drug treatment, and surgery groups. The reproducibility of our findings was confirmed by at least three independent experiments. Data are shown as mean ± standard error of the mean (SEM). For multiple comparisons, analyses of variance with Dunnett's *post hoc* tests or Tukey–Kramer tests were performed as appropriate. A *t*-test was used for comparison between two groups. The calculations were performed using GraphPad Prism version 9. The images were analysed and quantified using Image J. The numerical source data is presented in Supplementary Data 1.

Data availability

Supplementary Data 1 contains the source data for the graphs in the main figures. Supplementary Fig. 4 contains the original uncropped blot images of the main figures. The other data supporting the findings of this study are available from the corresponding author upon reasonable request.

Received: 9 May 2024; Accepted: 2 May 2025;

Published online: 08 May 2025

References

- Guo, Y. & Pu, W. T. Cardiomyocyte maturation. *Circ. Res.* **126**, 1086–1106 (2020).
- Ellingsen, O. et al. Molecular regulation of cardiomyocyte maturation. *Curr. Cardiol. Rep.* **27**, 32 (2025).
- Cho, G. S. et al. Neonatal transplantation confers maturation of PSC-derived cardiomyocytes conducive to modelling cardiomyopathy. *Cell Rep.* **18**, 571–582 (2017).
- Hill, J. A. & Olson, E. N. Cardiac plasticity. *N. Engl. J. Med.* **358**, 1370–1380 (2008).
- Coste, B. et al. PIEZO1 and PIEZO2 are essential components of distinct mechanically activated cation channels. *Science* **330**, 55–60 (2010).
- Coste, B. et al. Piezo proteins are pore-forming subunits of mechanically activated channels. *Nature* **483**, 176–181 (2012).
- Ge, J. et al. Architecture of the mammalian mechanosensitive PIEZO1 channel. *Nature* **527**, 64–69 (2015).
- Zhao, Q. et al. Structure and mechanogating mechanism of the PIEZO1 channel. *Nature* **554**, 487–492 (2018).
- Jiang, F. et al. The mechanosensitive PIEZO1 channel mediates heart mechano-chemo transduction. *Nat. Commun.* **12**, 869 (2021).
- Yu, Z.-Y. et al. PIEZO1 is the cardiac mechano-sensor that initiates the cardiomyocyte hypertrophic response to pressure overload in adult mice. *Nat. Cardiovasc. Res.* **1**, 577–591 (2021).

11. Sharif-Naeini, A. et al. TRP channels and mechanosensory transduction: insights into the arterial myogenic response. *Eur. J. Physiol.* **456**, 529–540 (2008).
12. Yue, Z. et al. Role of TRP channels in the cardiovascular system. *Am. J. Physiol. Heart Circ. Physiol.* **308**, H157–H182 (2015).
13. Numaga-Tomita, T. et al. TRPC3-GEF-H1 axis mediates pressure overload-induced cardiac fibrosis. *Sci. Rep.* <https://doi.org/10.1038/srep39383> (2016).
14. Oda, S. et al. TRPC6 counteracts TRPC3-Nox2 protein complex leading to attenuation of hyperglycemia-induced heart failure in mice. *Sci. Rep.* <https://doi.org/10.1038/s41598-017-07903-4> (2016).
15. Zou, Y. et al. Activation of transient receptor potential vanilloid 4 is involved in pressure overload-induced cardiac hypertrophy. *eLife* **11**, e74519 (2022).
16. Muraki, K. et al. TRPV2 is a component of osmotically sensitive cation channels in murine aortic myocytes. *Cir. Res.* **93**, 829–838 (2003).
17. Iwata, Y. et al. A novel mechanism of myocyte degeneration involving the Ca²⁺-permeable growth factor-regulated channel. *J. Cell Biol.* **161**, 957–967 (2003).
18. Katanosaka, Y. et al. TRPV2 is critical for the maintenance of cardiac structure and function in mice. *Nat. Commun.* **5**, 3932 (2014).
19. Rubinstein, J. et al. Novel role of transient receptor potential vanilloid 2 in the regulation of cardiac performance. *Am. J. Physiol. Heart Circ. Physiol.* **306**, H574–H584 (2014).
20. Ujihara, Y. et al. Induced NCX1 overexpression attenuates pressure overload-induced pathological cardiac remodeling. *Cardiovasc. Res.* **111**, 348–361 (2016).
21. Ujihara, Y. et al. Elimination of fukutin reveals cellular and molecular pathomechanisms in muscular dystrophy-associated heart failure. *Nat. Commun.* **10**, 5754 (2019).
22. Qu, Y. et al. Gene expression of Na⁺/Ca²⁺ exchanger during development in human heart. *Cardiovasc. Res.* **45**, 866–873 (2000).
23. Qu, Y. & Boutjdir, M. Gene expression of SERCA2a and L- and T-type Ca²⁺ channels during human heart development. *Pediatr. Res.* **50**, 569–574 (2001).
24. Munoz, J. P. et al. The transcription factor MEF2c mediates cardiomyocyte hypertrophy induced by IGF-1 signalling. *Biochem. Biophys. Res. Commun.* **388**, 155–160 (2009).
25. Zhang, C. L. et al. Class II histone deacetylase act as signal-responsive repressor of cardiac hypertrophy. *Cell* **110**, 479–488 (2002).
26. Guo, Y. et al. Hierarchical and stage-specific regulation of murine cardiomyocyte maturation by serum response factor. *Nat. Commun.* **9**, 3837 (2018).
27. Macvanin, M. et al. New insights on the cardiovascular effects of IGF-1. *Front. Endocrinol.* **14**, 1142644 (2023).
28. Shyu, K.-G. et al. Insulin-like growth factor-1 mediates stretch-induced upregulation of myostatin expression in neonatal rat cardiomyocytes. *Cardiovasc. Res.* **68**, 405–414 (2005).
29. Bevan, A. K. et al. Early heart failure in the SMNΔ7 model of spinal muscular atrophy and correction by postnatal scAAV9-SMN delivery. *Hum. Mol. Genet.* **19**, 3895–3905 (2010).
30. Kitaoka, H. et al. Low dose dobutamine stress echocardiography predicts the improvement of ventricular systolic function in dilated cardiomyopathy. *Heart* **81**, 523–527 (1999).
31. Ayuzawa, N. et al. Rac1-mediated activation of mineralocorticoid receptor in pressure overload-induced cardiac injury. *Hypertension* **67**, 99–106 (2016).
32. McCain, M. L. & Parker, K. K. Mechanotransduction: the role of mechanical stress, myocyte shape, and cytoskeletal architecture on cardiac function. *Pflug. Arch.* **462**, 89–104 (2011).
33. Maillet, M., Berlo, J. H. V. & Molkentin, J. D. Molecular basis of physiological heart growth: fundamental concepts and new players. *Nat. Rev. Mol. Cell Biol.* **14**, 38–48 (2013).
34. Carlos-Oliveira, M. et al. Current strategies of mechanical stimulation for maturation of cardiac microtissues. *Biophys. Rev.* **13**, 717–727 (2021).
35. Zhang, X. et al. Cardiomyopathy in transgenic mice with cardiac-specific overexpression of serum response factor. *Am. J. Physiol. Heart Circ. Physiol.* **280**, H1782–H1792 (2001).
36. Zhang, X. et al. Early postnatal cardiac changes and premature death in transgenic mice overexpressing a mutant form of serum response factor. *J. Biol. Chem.* **276**, 40033–40040 (2001).
37. Parlakian, A. et al. Temporally controlled onset of dilated cardiomyopathy through disruption of the SRF gene in adult heart. *Circulation* **112**, 2930–2939 (2005).
38. Wang, X. & Gerdes, A. M. Chronic pressure overload cardiac hypertrophy and failure in guinea pigs: III. Intercalated disc remodeling. *J. Mol. Cell Cardiol.* **31**, 333–343 (1999).
39. Vermij, S. H., Abriel, H. & Veen, T. A. B. Refining the molecular organization of the cardiac intercalated disc. *Cardiovasc. Res.* **113**, 259–275 (2017).
40. Wilson, A. J. et al. Cardiomyocyte growth and sarcomerogenesis at the intercalated disc. *Cell Mol. Life Sci.* **71**, 165–181 (2013).
41. Andersson, K. B. et al. Moderate heart dysfunction in mice with inducible cardiomyocyte-specific excision of the Serca2 gene. *J. Mol. Cell Cardiol.* **47**, 180–187 (2009).
42. Louch, W. E. et al. Sodium accumulation promotes diastolic dysfunction in end-stage heart failure following Serca2 knockout. *J. Physiol.* **588**, 465–478 (2010).
43. Swift, F. et al. Extreme sarcoplasmic reticulum volume loss and compensatory T-tubule remodeling after Serca2 knockout. *Proc. Natl Acad. Sci. USA* **109**, 3997–4001 (2012).
44. Boardman, N. T. et al. Impaired left ventricular mechanical and energetic function in mice after cardiomyocyte-specific excision of Serca2. *Am. J. Physiol. Heart Circ. Physiol.* **306**, H1018–H1024 (2014).
45. Gluckman, P. D. & Butler, J. H. Parturition-related changes in insulin-like growth factors-I and -II in the perinatal lamb. *J. Endocrinol.* **99**, 223–232 (1983).
46. Daughaday, W. H. et al. Measurement of somatomedin-related peptides in fetal, neonatal, and maternal rat serum by insulin-like growth factor (IGF)-I radioimmunoassay, IGF-II radioreceptor assay (RRA), and multiplication-stimulating activity RRA after acid-ethanol extraction. *Endocrinology* **110**, 575–581 (1982).
47. Bianca, C. B., Kate, L. W., Lynette, P. & Julie, R. M. Molecular distinction between physiological and pathological cardiac hypertrophy: Experimental findings and therapeutic strategies. *Pharmacol. Ther.* **128**, 191–227 (2010).
48. Takeda, N. et al. Cardiac fibroblasts are essential for the adaptive response of the murine heart to pressure overload. *J. Clin. Invest.* **120**, 254–265 (2010).
49. Cao, P., Maximov, A. & Sudhof, T. C. Activity-dependent IGF-1 exocytosis is controlled by the Ca²⁺-sensor synaptotagmin-10. *Cell* **145**, 300–311 (2011).
50. Fukuda, R. et al. Mechanical force regulate cardiomyocyte myofilament maturation via the VCL-SSH1-CFL axis. *Dev. Cell.* **51**, 62–77 (2019).
51. Mahony, L. Maturation of calcium transport in cardiac sarcoplasmic reticulum. *Pediatr. Res.* **24**, 639–643 (1988).
52. Katanosaka, K. et al. TRPV2 is required for mechanical nociception and the stretch-evoked response of primary sensory neurons. *Sci. Rep.* **8**, 16782 (2018).
53. Nakamoto, H. et al. Involvement of transient receptor potential vanilloid channel 2 in the induction of lubricin and suppression of ectopic endochondral ossification in mouse articular cartilage. *Arthritis Rheumatol.* **73**, 1441–1450 (2021).
54. Park, U. et al. TRP vanilloid knock-out mice are susceptible to perinatal lethality but display normal thermal and mechanical nociception. *J. Neurosci.* **31**, 11425–11436 (2011).

55. O'Connor, B., Robbins, N., Kosh, S. & Rubinstein, J. TRPV2 channel-based therapies in the cardiovascular field. Molecular underpinnings of clinically relevant therapies. *Prog. Biophys. Mol. Biol.* **159**, 118–125 (2021).
56. Koch, S. E. et al. Transient receptor potential vanilloid 2 function regulates cardiac hypertrophy via stretch-induced activation. *J. Hypertens.* **35**, 602–611 (2017).
57. Bersell, K. et al. Moderate and high amounts of tamoxifen in aMHC-MerCreMer mice induce a DNA damage response, leading to heart failure and death. *Dis. Model. Mech.* **6**, 1459–1469 (2013).
58. Koitabashi, N. et al. Avoidance of transient cardiomyopathy in cardiomyocyte-targeted tamoxifen-induced MerCreMer gene deletion models. *Circ. Res.* **105**, 12–15 (2009).
59. Katanosaka, Y. et al. Calcineurin inhibits Na⁺/Ca²⁺ exchange in phenylephrine-treated hypertrophic cardiomyocytes. *J. Biol. Chem.* **280**, 5764–5772 (2005).

Acknowledgements

This work was supported by Grants-in-Aid from the Ministry of Education, Culture, Sports, Science, and Technology of Japan (grant numbers 23722538, 23722773 and 23777371 to Y.K., 22562791 to K.K., and 23722363 to Y.U.), the Japan Society for the Promotion of Science (Funding Program for Next Generation World-Leading Researchers [NEXT Program] to Y.K.), and the Japan Agency for Medical Research and Development (AMED PRIME to Y.K.). This work was supported in part by a grant from the Suzuken Memorial Foundation, Mitsubishi Foundation, and Takeda Science Foundation to Y.K. We thank the China Scholarship Council for the scholarships of Y.D. (202108210109) and Y.C. (202108050035).

Author contributions

Y.D. performed most experiments under the supervision of Y.K. Y.K. planned, designed, and supervised the study and wrote the paper. G.W., Y.U., Y.C., M.Y., Kazu.N., and K.K. carried out the experiments and analysed data. Kei.N. gave conceptual advice.

Competing interests

The authors declare no competing interests.

Additional information

Supplementary information The online version contains supplementary material available at <https://doi.org/10.1038/s42003-025-08167-9>.

Correspondence and requests for materials should be addressed to Yuki Katanosaka.

Peer review information *Communications Biology* thanks Eleonora Cianflone and the other, anonymous, reviewer(s) for their contribution to the peer review of this work. Primary Handling Editors: Daniele Torella and Dario Ummarino. A peer review file is available.

Reprints and permissions information is available at <http://www.nature.com/reprints>

Publisher's note Springer Nature remains neutral with regard to jurisdictional claims in published maps and institutional affiliations.

Open Access This article is licensed under a Creative Commons Attribution-NonCommercial-NoDerivatives 4.0 International License, which permits any non-commercial use, sharing, distribution and reproduction in any medium or format, as long as you give appropriate credit to the original author(s) and the source, provide a link to the Creative Commons licence, and indicate if you modified the licensed material. You do not have permission under this licence to share adapted material derived from this article or parts of it. The images or other third party material in this article are included in the article's Creative Commons licence, unless indicated otherwise in a credit line to the material. If material is not included in the article's Creative Commons licence and your intended use is not permitted by statutory regulation or exceeds the permitted use, you will need to obtain permission directly from the copyright holder. To view a copy of this licence, visit <http://creativecommons.org/licenses/by-nc-nd/4.0/>.

© The Author(s) 2025